Supplementary Data

Supplementary Materials

Brainstem nuclei of the ascending arousal and autonomic systems: labeling and tissue properties

Labels of the raphe nuclei. We generated labels of three raphe nuclei: the raphe magnus (RMg), the median raphe (MnR), and the dorsal raphe (DR). The RMg and the MnR appeared as islands of low-diffusion fractional anisotropy (FA) surrounded by white matter (WM) fiber bundles. Identification of the RMg coincided with anatomical histological location (Paxinos and Huang, 1995; Paxinos et al., 2012) (namely rostrodorsal to the inferior olivary nuclei [ION]). The MnR label was in the brainstem midline, ventral to the DR and medial to the superior cerebellar peduncle, consistent with *ex vivo* atlases (Paxinos and Huang, 1995; Paxinos et al., 2012); nevertheless, on visual inspection, its location in our *in vivo* magnetic resonance imaging (MRI) images (at the midbrain-pontine junction) appeared slightly rostral to what has been reported in two-dimensional *ex vivo* atlas plates (Paxinos and Huang, 1995; Paxinos et al., 2012). Currently, a precise comparison is hampered by differences between *in vivo* and *ex vivo* methodologies (e.g., a different slice orientation with respect to the long medullary-pontine axis) and the lack of a common spatial coordinate system. Given the small size of the RMg and MnR, further validation studies with histologic-radiologic correlations are needed to elucidate whether more than one nucleus pertains to each label provided in this work. The DR displayed a similar T2-weighted signal compared with the periaqueductal gray (PAG) and higher T2-weighted signal compared with neighboring regions (e.g., the colliculi). Interestingly, the density of directionally oriented fibers was higher in the DR than in the PAG, an observation that enabled the automatic separation of the DR from the PAG based on FA values. Notably, there are major cytological differences between these two nuclei (Olszewski and Baxter, 1982) that might underlie the observed MRI contrast. The DR is made up of relatively densely packed, very large neurons, whereas the PAG comprises very small neurons.

PAG label. This label likely contains the PAG only, a structure that surrounds the aqueduct of Sylvius. The PAG does not completely encircle the aqueduct, with the DR occupying the midline ventral to the aqueduct (Linnman et al., 2012). In this work, we provided a novel *in vivo* procedure to automatically identify the borders between the PAG and the DR on the basis of the content of oriented fibers underlying differences in FA values (higher in the DR than in the PAG). The tissue properties of the PAG and the DR underlying the observed MRI contrast are discussed in the Labels of the Raphe Nuclei section. Given a high spatial variability of individual peaks reported in the literature for the PAG location in humans (Linnman et al., 2012), we foresee that the PAG label provided by this study may improve the localization of the PAG in *in vivo* MRI. In turn, this will aid localization of lesions affecting the PAG and will facilitate anatomical and functional investigations of PAG connectivity in conditions such as pain, migraine headache, opioid addiction, disorders of consciousness, and emotional dysregulation (Satpute et al., 2013).

Brainstem nuclei of the motor system: labeling and tissue properties

ION label. This label likely contains the three subdivisions of the ION: the principal, the medial, and the dorsal nuclei of the inferior olive (Armstrong et al., 1999; Paxinos et al., 2012). On the basis of the label shape and image resolution, part of the amiculum of the olive (which is a capsule of incoming fibers from the cerebral cortex, other brainstem

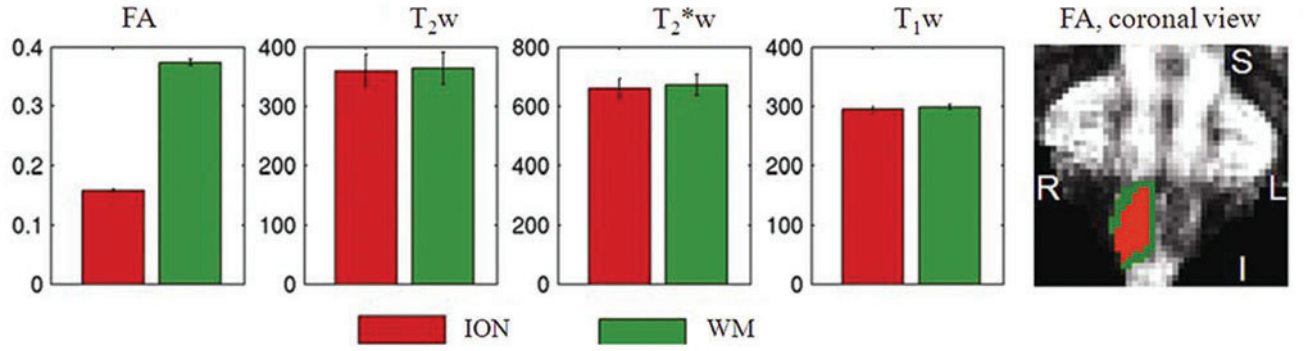

SUPPLEMENTARY FIG. S1. Magnetic resonance imaging contrast for delineation of brainstem inferior olivary nuclei (ION). For fractional anisotropy (FA), T2-, T2*-, and T1-weighted images, we show the bar (error-bar) plot of the group average (SE) of the signal (mean across voxels) in the right ION (red) and in a neighboring white matter (WM) region (green), obtained by dilating the ION region and excluding voxels pertaining to the CSF mask (see green ring around the ION, in red, in the right panel). The % contrast for the ION (computed for each subject as the ratio between the difference and the sum of the signal in the ION and in the WM region) was much higher in FA images ($40.6\% \pm 1.0\%$) than in T2-, T2*-, and T1-weighted images ($0.7\% \pm 0.3\%$, $0.9\% \pm 0.6\%$, and $0.8\% \pm 0.3\%$, respectively).

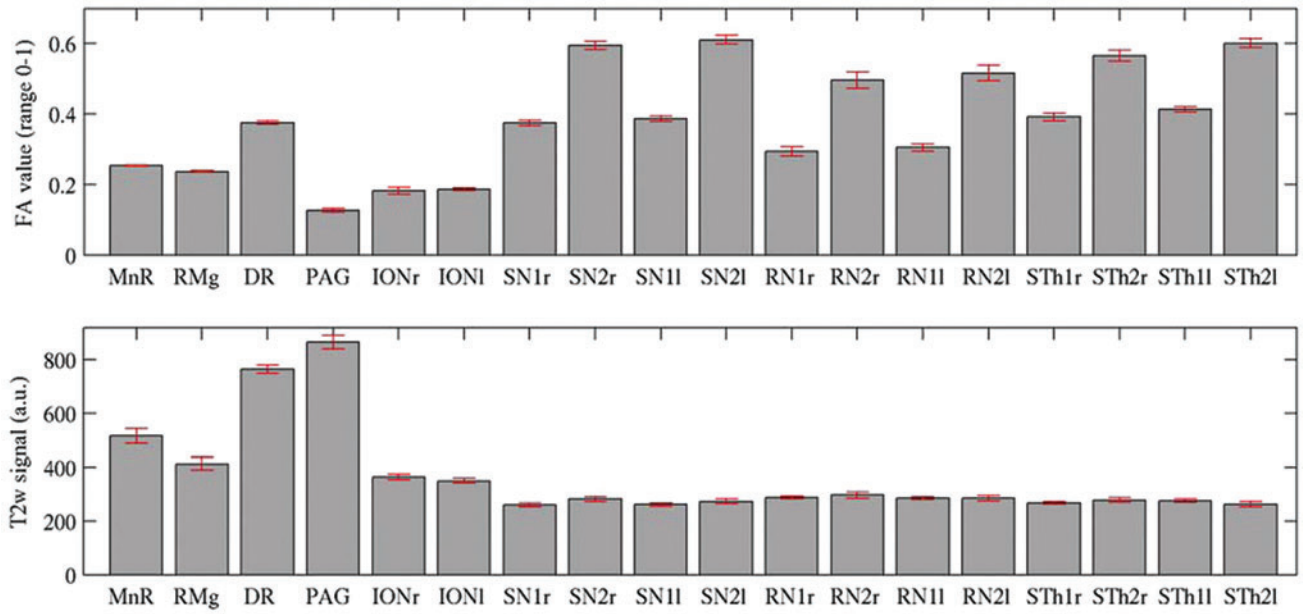

SUPPLEMENTARY FIG. S2. Region-based analysis of FA and T2-weighted values in brainstem nuclei (Bn). The bar (error bar) plot displays the group average (SE) of the FA and T2-weighted values (mean across voxels) in each identified Bn and each subregion of the substantia nigra (SN), red nucleus (RN), and subthalamic nucleus (STh; right, left indicated with r, l; subregions indicated with 1, 2). We did not observe any significant signal change between left and right regions/subregions. It should be noted that T2-weighted values in the dorsal raphe (DR) and the periaqueductal gray (PAG) were higher than those in the other identified Bn, and that the PAG had lower FA values than the DR. Interestingly, FA also varied between the two subregions of the SN, RN, and STh.

sites, and the spinal cord) is likely located within the ION label, probably because of partial volume effects. The ION label displays lower FA and similar T2 values compared with large neighboring WM fiber bundles, likely indicating lower myelin content and similar iron content between the ION and the surrounding WM.

Substantia nigra label. Substantia nigra (SN) consists of two parts with different connections and functions: the pars compacta (SNC) and pars reticulata (SNR). Our *in vivo* multi-contrast methodology allowed us to identify [as in previous work, Xiao et al. (2014)] the entire SN on the basis of the T2-weighted contrast, likely due to a high iron content of the SN (Snyder and Connor, 2009). In addition, we were able to segregate two subregions of the SN, an area displaying a higher diffusion FA neighboring an area with a lower diffusion FA, which we tentatively attributed, respectively, to SNC and SNR. This attribution is compatible with histological studies of the SN (Francois et al., 1999), which report that neurons of the SNC have particularly long and thick dendrites, and that neurons in the SNR are much less densely packed than those in the SNC. We identified several islands of SN2 (the subregion compatible with SNC), one large area medial to SN1 (SN2-medial), and another lateral to SN1 and superior to SN2-medial. This result is also qualitatively consistent with *ex vivo* human atlases (Paxinos et al., 2012), which report the existence of several SNC areas, which sometimes divide or envelope the SNR (Paxinos et al., 2012). Interestingly, previous *in vivo* studies segmented the SN into two subregions based on their anatomical connectivity to the striatum (Chowdhury et al., 2013) or to the whole brain (Menke et al., 2010). Further investigation is needed to elucidate the relationship between our results and previous subdivisions of the SN. The volume of the SN reported in this work ($\sim$490 mm^3 on average between SNl and SNr) is comparable with that reported in a previous *in vivo* work ($\sim$450–520 mm^3, Chowdhury et al., 2013; Menke et al., 2010), although other *in vivo* studies report lower values ($\sim$250 mm^3, Keuken et al., 2014; Kwon et al., 2012; Xiao et al., 2014), and higher values are found postmortem ($\sim$678 mm^3, von Bonin and Shariff, 1951). This variability in SN volume across studies might reflect differences in methodology and/or image contrasts used.

Red nucleus label. Due to the high iron content (Paxinos et al., 2012), the red nucleus (RN) has been previously identified on T2-weighted images at lower field strengths [see, for instance, Xiao et al. (2014)] as a hypointense region. The volume of the total RN reported in this work ($\sim$240 mm^3 on average between RNl and RNr) falls within the range of previously reported values ($\sim$200–280 mm^3, Keuken et al., 2014; Xiao et al., 2014). This nucleus can be divided into two histologically distinct structures, a caudal magnocellular (RNm) part and a rostral parvocellular (RNp) part, with a size-related dominance of the RNp and a marked regression of the RNm in humans (Paul and Gould, 2010). In this study, we identified two subregions of the RN, each occupying $\sim$50% of its volume (see Table 1), with a different content of oriented fibers and a similar T2-weighted signal (see Supplementary Fig. S2). Previous work (Duvernoy, 1999)

reports a subdivision of the RN on the basis of vascular density, with a more densely vascularized region surrounding a poorly vascularized central region with the shape of a crescent. Notably, because of their similar relative size, it seems unlikely that these subdivisions [both the ones presented in this report and in Duvernoy (1999)] reflect the RNm and the RNp [in humans, RNm is much smaller than RNp (Paul and Gould, 2010; Paxinos et al., 2012; Stern, 1938)], and further *ex vivo* work might elucidate the relationship between our and previous findings (Duvernoy, 1999), also with respect to RNm and RNp.

Subthalamic nucleus label. The subthalamic nucleus (STh) is a small, bi-convex, lens-shaped subcortical structure. Although it pertains to the diencephalon, we also report our findings on the STh, because it shares some anatomical boundaries with the SN and also, similar to the SN, the STh is a nodal component of the basal ganglia. We defined an STh label of $\sim 160\,\mathrm{mm}^3$, comparable to previous work ($\sim 155\,\mathrm{mm}^3$, Lambert et al., 2012; Xiao et al., 2014 and $\sim 170\,\mathrm{mm}^3$ in Accolla et al., 2014). Other *in vivo* work (Keuken et al., 2014) reports instead a $\sim 55\,\mathrm{mm}^3$ volume. Interestingly, we automatically identified two subregions—dorsomedial and ventrolateral ellipsoidal-shaped sub-layers—with higher and lower FA, respectively, which might reflect different geometry of the ellipsoidal-shaped dendritic arborization within the STh (Yelnik and Percheron, 1979). The STh is subdivided into three different functional territories: a large motor territory, a smaller associative (oculomotor, cognitive) territory, and a medial limbic tip (Accolla et al., 2014; Benarroch, 2008). Further work is needed to elucidate the relationship between the structural subdivisions of the STh provided in this work and the functional subregions previously reported. In turn, this may facilitate more precise targeting of STh subregions for deep brain stimulation therapy.